Neuron, Vol. 37, 311–322, January 23, 2003, Copyright ©2003 by Cell Press

Mechanisms of Gamma Oscillations in the Hippocampus of the Behaving Rat

Jozsef Csicsvari,[1] Brian Jamieson,[2] Kensall D. Wise,[2] and György Buzsáki[1,*]
[1]Center for Molecular and Behavioral Neuroscience
Rutgers, The State University of New Jersey
197 University Avenue
Newark, New Jersey 07102
[2]Department of Electrical Engineering and Computer Science
The University of Michigan
Ann Arbor, Michigan 48109

Summary

Gamma frequency oscillations (30–100 Hz) have been suggested to underlie various cognitive and motor functions. Here, we examine the generation of gamma oscillation currents in the hippocampus, using two-dimensional, 96-site silicon probes. Two gamma generators were identified, one in the dentate gyrus and another in the CA3-CA1 regions. The coupling strength between the two oscillators varied during both theta and nontheta states. Both pyramidal cells and interneurons were phase-locked to gamma waves. Anatomical connectivity, rather than physical distance, determined the coupling strength of the oscillating neurons. CA3 pyramidal neurons discharged CA3 and CA1 interneurons at latencies indicative of monosynaptic connections. Intrahippocampal gamma oscillation emerges in the CA3 recurrent system, which entrains the CA1 region via its interneurons.

Introduction

Oscillations in cortical structures are believed to provide temporal windows that bind coherently cooperating neuronal assemblies for the representation, processing, storage, and retrieval of information (cf. Engel et al., 2001; Traub et al., 1999; Buzsáki et al., 1994). Of the large family of brain oscillatory patterns, gamma oscillations have received special attention because of their alleged role in sensory binding (Singer, 1993; Gray, 1994), memory (Fell et al., 2001), attentional selection (Fries et al., 2001a), and "conscious" experience (Llinás et al., 1998; Varela et al., 2001). Gamma oscillations are also prevalent in the hippocampal formation, where they have been proposed to assist in encoding and retrieval of memory traces (Bragin et al., 1995; Lisman and Idiart, 1995; Chrobak and Buzsáki, 1998; Hasselmo et al., 1996).

In contrast to sensory cortical regions, where gamma waves are induced by sensory stimulations (Gray et al., 1989; Eckhorn, 1994; but see Roelfsema et al., 1997; Fetz et al., 2000; Fries et al., 2001b), the conditions that give rise to the persistent hippocampal gamma oscillations (Stumpf, 1965; Buzsáki et al., 1983; Leung, 1992; Soltész and Déschenes, 1993; Hirai et al., 1999) are not known. In vivo, they have been described in the dentate and CA1 regions (Leung, 1979; Buzsáki et al., 1983; Bragin et al., 1995; Charpak et al., 1995; Penttonen et al., 1998), but much less is known about gamma oscillations in the CA3 hippocampal region. This information is critical because although both dentate and CA3 principal cells are innervated by the axon collaterals of layer II entorhinal cortical neurons (Tamamaki and Nojyo, 1993), the CA3 region has been postulated to generate gamma oscillations independent of cortical inputs (Bragin et al., 1995; Fisahn et al., 1998).

Various in vitro models of gamma patterns have been tested to gain insight into the cellular-synaptic properties of gamma oscillations. Tetanus- or drug-induced oscillations in the gamma band have been described in each hippocampal region in vitro (Whittington et al., 1995, 1997, 2001; Traub et al., 1996; Colling et al., 1998; Stanford et al., 1998; Stenkamp et al., 2001; Towers et al., 2002; Fisahn et al., 1998, 2002), and putative mechanisms for the generation of gamma oscillations have been offered by computer models (Leung, 1982, 1998; Wang and Buzsáki, 1996; Traub et al., 1996, 1997, 2001; Jensen and Lisman, 1996; Wallenstein and Hasselmo, 1997; Chow et al., 1998; White et al., 1998; Orban et al., 2001; Tiesinga et al., 2001). However, it is not known to what extent these models reflect gamma oscillation mechanisms in the intact brain and how the postulated mechanisms interact with each other during behavior. Persistent (carbachol- and kainate-induced) gamma oscillations require an intact CA3 region (Fisahn et al., 1998), whereas transient, tetanus-induced gamma oscillation can be elicited in the CA1 but not in the CA3 region (Whittington et al., 1995, 1997). Furthermore, the various models provide different predictions about the timing of principal cells and interneurons and their relationship to the extracellular field. Finally, various theoretical models postulate conflicting requirements for interregional synchronization (Lisman, 1998; Rolls, 1996). Quantitative evaluation of these issues in the behaving animal requires simultaneous recording of gamma currents from the various subregions along with concurrently recorded neurons from each of these regions. To examine the interregional relationships of gamma oscillations and the network mechanisms of their generation, we used two-dimensional silicon probes with a large number of recording sites in freely moving rats (Csicsvari et al., 2001).

Results

In structures with regularly arranged neurons and afferents, such as the various layers of the hippocampus, extracellularly recorded currents provide information about location of currents flowing into and out of neurons. Simultaneously recorded extracellular unit activity can assist in the interpretation of currents, i.e., whether they are induced by coherent afferent activity and/or intrinsic membrane properties or reflect passive, "return" currents. In the present studies, local field potentials (i.e., voltage changes) were recorded simultaneously from 96

*Correspondence: buzsaki@axon.rutgers.edu

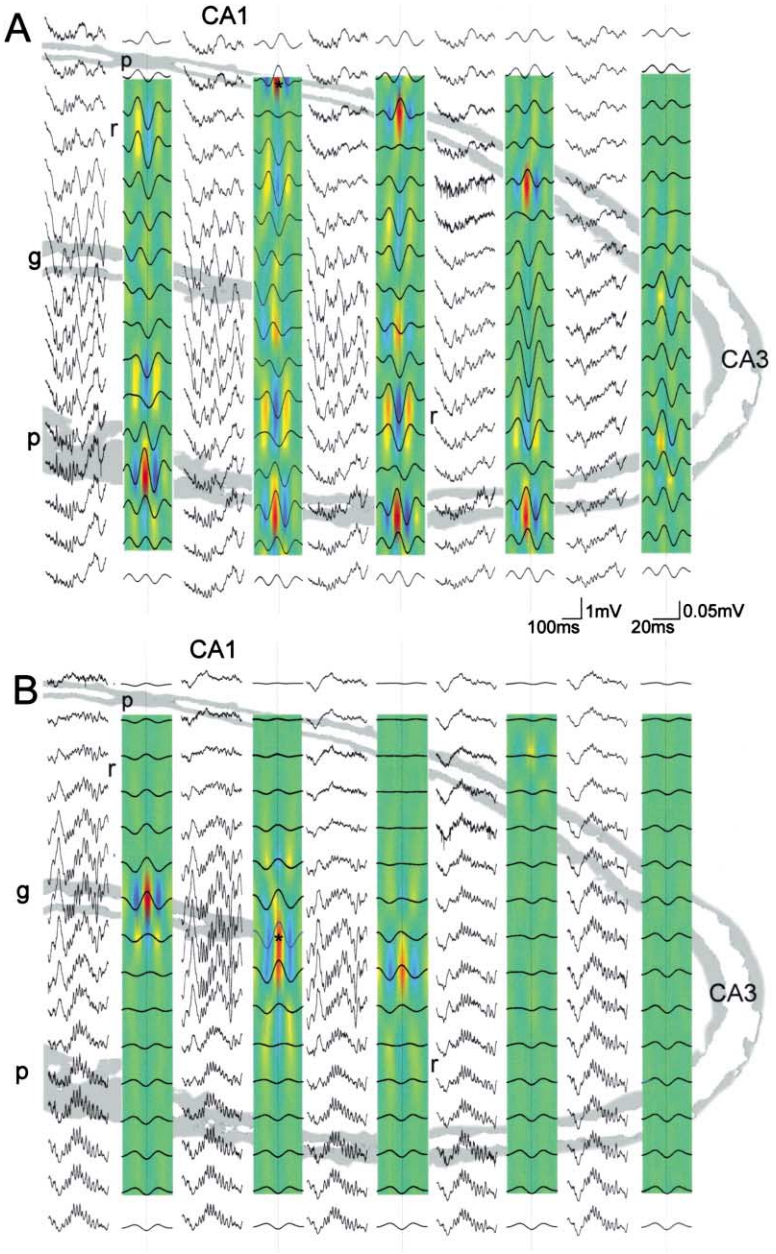

Figure 1. Gamma Oscillatory Patterns in the Hippocampus during REM Sleep

Two sets of single epochs (300 ms voltage traces; 1 Hz–3 kHz) of simultaneously recorded field potentials from five shanks (300 μm distance between shanks) of the silicon probe (each shank had 16 recording sites at 100 μm vertical spacing) are shown. The sixth shank penetrated lateral to the CA3b pyramidal layer (data not shown). Color panels: averaged gamma field potentials (30–80 Hz; $n > 1000$ gamma epochs for each voltage trace) and the derived CSD maps. Hot and cold colors correspond to sources and sinks, respectively. The center of the averaged field gamma traces (superimposed on the CSD plots) corresponds to the recording sites. The corresponding single epochs are displaced to the left (note the difference in time and amplitude calibrations for single epochs and averages). Either a CA1 pyramidal layer site (A) or a GC layer site (B) served as a reference for averaging gamma epochs >2 SD at the reference site (asterisks; vertical lines). The weak gamma currents in the rightmost shank in (A) are due to the oblique spacing of the recording sites relative to cell orientation. Note the absence of sink-source pairs in the CA1 pyramidal layer in (B). p, pyramidal layer; g, GC layer; r, stratum radiatum. The position of recording sites was determined from the evoked potentials in response to commissural and perforant path input stimulation and from the histological sections containing the probe.

sites in 6 freely moving rats. The 2-dimensional arrangement of the recording sites in the frontal plane allowed for the monitoring of field potentials in the major hippocampal regions (Figure 1). The location of each recording position was determined by the evoked potentials in response to stimulation of the perforant path and commissural inputs combined with histological verification of probe tracks (Bragin et al., 1995). The recorded voltages were converted to current-source densities (CSD) to eliminate volume conduction of the voltage fields in the extracellular medium. Because the distance between the recording sites of the probe (100 μm) could not reliably separate individual neurons (Gray et al., 1995; Harris et al., 2000), the relationship between gamma field and unit activity was examined in an additional six rats using independently movable wire tetrodes (Csicsvari et al., 2001). The time relationship between gamma currents was measured directly or estimated indirectly from the relative phase differences between regions using frequency domain analysis. The relative timing of currents and unit activity was referenced to gamma waves recorded in the CA1 pyramidal layer, unless noted otherwise. Group data were calculated from sessions of 10–15 min during sleep, waking immobility, and walking.

Distribution of Gamma Currents in the Dentate-CA3-CA1 Regions

We first addressed the amplitude and phase relationships of gamma waves in the dentate gyrus, CA3, and CA1 regions of the hippocampus. Two short gamma oscillation episodes (1 Hz–5 kHz), recorded during REM sleep, are illustrated in Figure 1. For determining the regional distribution of gamma oscillation-associated

currents, the field (voltage) traces were first filtered (30–80 Hz), and the peaks of the filtered gamma waves (threshold $>$ 2 SD from baseline mean), recorded from either the CA1 pyramidal layer or the granule cell (GC) layer (reference sites), were used to construct gamma cycle averages. The mean voltage traces were then used to construct one-dimensional CSD maps for each shank. The average wavelengths of the gamma waves were similar in the two regions (CA1: 18.8 $\pm$ 0.11 ms; GC: 18.9 $\pm$ 0.21; $p > 0.3$; i.e., approximately 53 Hz; $n = 6$ rats). Gamma waves showed a phase reversal at the border of strata radiatum and pyramidale in both CA1 and CA3 regions, associated with current sources (red in CSD maps) in the pyramidal layer flanked by a larger sink (blue) in stratum radiatum and a smaller one in stratum oriens/alveus. The current source maximum preceded the positive peak of the local field (voltage) by 0.73 $\pm$ 0.09 ms in the CA1 pyramidal layer ($n = 21$ sites in 6 rats). The source maximum in the CA3 pyramidal layer occurred 1.36 $\pm$ 0.15 ms earlier than in the CA1 pyramidal layer ($n = 96$ pairs in 6 rats). The current source in the GC layer, associated with the CA1 reference gamma waves, was relatively small (Figure 1A). In contrast, when the GC layer was used as the reference, gamma waves reversed across the GC layer associated with a large current source in this layer but not in the CA3-CA1 regions (Figure 1B).

The use of CSD traces, instead of the extracellular voltage field, also allowed us to remove spurious coherence due to volume conduction of the field potentials. Coherence values of gamma currents were highest between a reference site in the CA1 pyramidal layer and other surrounding CA1 sites (Figures 2A and 2C; $n = 140$ pairs), followed by pairs between CA1 and CA3 sites ($n = 278$), and the lowest values were observed between the CA1 pyramidal layer and GC layer of the dentate gyrus ($n = 161$; $p < 0.001$; ANOVA tests). In agreement with the time domain analysis (Figure 1), gamma currents recorded in the CA3-CA1 pyramidal layer were in-phase (27.3° $\pm$ 7.5° with CA3 leading; i.e., 1.5 ms delay at 53 Hz) and out-of-phase with signals recorded in stratum radiatum of CA3-CA1 (CA1: 160.6° $\pm$ 8.3°; CA3: 203.9° $\pm$ 8.1°; Figure 2E). When the dentate GC layer was chosen as the reference site, coherent signals ($>$0.3) were observed within the dentate gyrus and between the granule cell layer and stratum lacunosum-moleculare (Figures 2B and 2D). Current signals recorded in the GC and molecular layers were phase reversed (Figure 2F). Gamma coherence between dentate gyrus and CA1 layers was lowest ($<$0.1), with somewhat larger values between current signals in dentate gyrus and CA3. These findings suggest that at least two gamma current generators reside in the hippocampal formation, one in the dentate gyrus and another one in the CA3-CA1 regions. They also indicate that gamma coherence does not simply decrease with distance (Bullock and McClune, 1989), but that the connectivity between the recording sites plays an important role.

Gamma Oscillations during Theta and Nontheta Epochs

In agreement with previous reports (Buzsáki et al., 1983; Leung, 1992, 1998), the power of field gamma oscillation in the CA1 region was larger during theta-associated behaviors ($p < 0.01$; paired t test). When gamma CSD rather than the voltage was used for comparison, the state-dependence of gamma power varied differentially in the different regions. On average, no significant differences in gamma CSD power between nontheta and theta epochs were observed in the CA1 strata pyramidale ($n = 63$ sites) and radiatum ($n = 73$) or CA3 strata pyramidale ($n = 96$) and radiatum ($n = 74$; for all tests, $p > 0.4$; paired t tests), but gamma currents were significantly larger (22.6%) during theta versus nontheta epochs in the GC layer ($p < 0.01$; $n = 134$). These findings indicate that the presence of theta oscillation is not a prerequisite for gamma oscillation, although gamma power is enhanced in the dentate gyrus during theta behavioral states. In addition, these findings further support the two-gamma generator hypothesis.

During theta epochs, the magnitude of gamma power varied as a function of the theta cycle in all regions. In the absence of theta, gamma epochs varied relatively irregularly, with no or low amplitude gamma currents alternating with "bursts" of gamma epochs that were considerably larger in amplitude than during theta. The difference in gamma oscillation dynamics in the two states is indicated quantitatively by the significantly larger coefficient of variation of gamma power during nontheta (CV = 0.36 $\pm$ 0.024 in CA1 [$n = 66$]; 0.34 $\pm$ 0.023 in CA3 [$n = 102$]; 0.38 $\pm$ 0.030 in GC [$n = 51$]) versus theta (CV = 0.27 $\pm$ 0.019 in CA1; 0.26 $\pm$ 0.013 in CA3; 0.29 $\pm$ 0.016 in GC) epochs (for all tests, $p < 0.005$; paired t tests).

Interregional Coupling of Gamma Oscillators

The low overall coherence values between currents in CA1 pyramidal layer and GC layer indicated that gamma oscillators in these respective regions are relatively independent. On the other hand, continuous display of gamma current power and coherence as a function of time suggested that the two generators do couple from time to time. Figure 3A shows a continuous display of gamma current magnitude (root mean square of the signal in consecutive 102 ms windows) recorded in the various cell layers. Power, as a function of time, fluctuated similarly within the CA1 region (Figure 3B; $r = 0.57 \pm 0.02$; $n = 140$ CA1 pairs in 6 rats). Gamma power fluctuation in the CA1 region also strongly correlated with power in CA3c ($r = 0.44 \pm 0.02$; $n = 102$) and progressively less so with CA3b ($r = 0.37 \pm 0.02$; $n = 30$) and CA3a (0.33 ± 0.02; $n = 57$) regions. All these correlations were significant (for all tests, $p < 0.001$). The least, but nevertheless still significant, correlation of power was observed between CA1 and the GC layers ($r = 0.24 \pm 0.01$, $p < 0.001$; $n = 161$). Coherence changes of gamma currents (gray traces in Figure 3A) in different regions faithfully reflected the changes in power correlations.

In addition to calculating correlations, a multilinear regression method was used to examine how well multiple sites in the CA3 pyramidal layer or GC layer predict the time-varying power changes in the CA1 region. A cross-validation method was used in these calculations. The regression equation was calculated for the first part of the recording session, and the correlation coefficient ("prediction") was calculated for the second half. The accuracy of prediction for a given CA1 site increased with the number of CA3 sites ($n = 1$ to 6; Figure 3C).

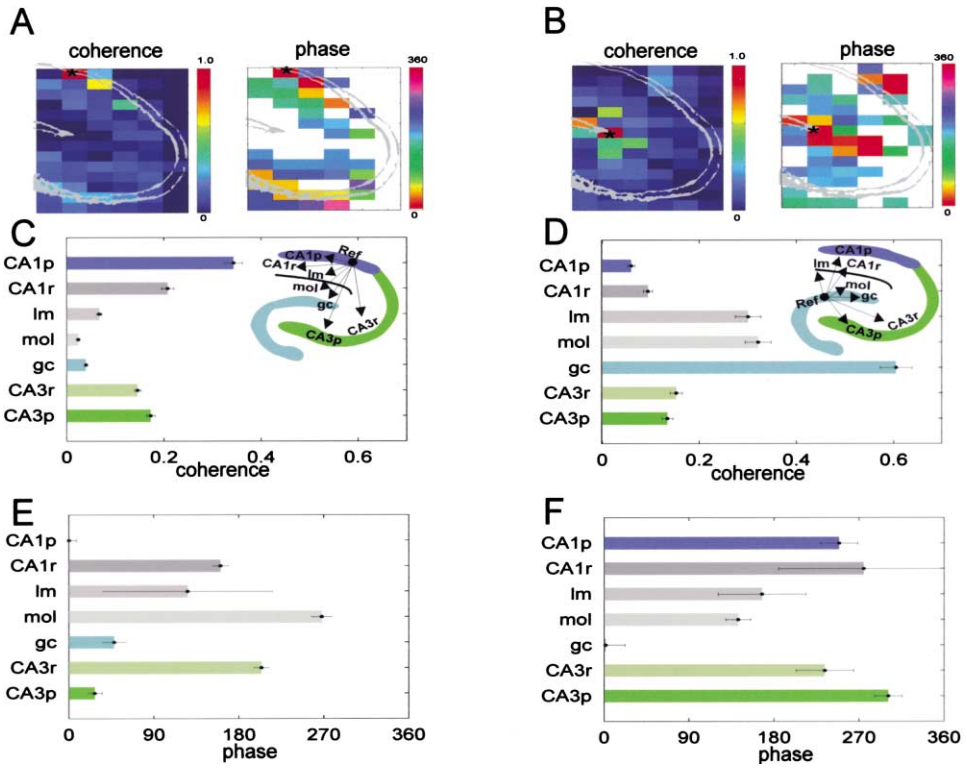

Figure 2. Coherence and Phase Maps of Gamma Oscillation Currents

(A and B) Single animal. Asterisk, reference site; color-coded rectangles, coherence and phase values of gamma currents. Phase values are shown only at sites with >0.1 coherence values. In (A), note that gamma currents are in phase in the CA1-CA3 pyramidal layers (with relatively high coherence values; light blue to red) and phase-reversed in stratum radiatum (compare blue-green to yellow-red). In (B), note the high coherence values and in-phase gamma currents mostly in the GC layer.

(C–F) Group data from different sites in six animals (mean ± SE; 10 min sleep epochs). Ref, reference site. Note similar phase in the CA1 and CA3 pyramidal layers (E) and out-of-phase currents in all layers outside the GC layer (F). Note also the low coherence values between CA1 pyramidal layer and GC layer (C and D). CA1p, CA3 p, pyramidal layer; CA1r, CA3r, stratum radiatum; GC, granule cell layer; lm, stratum lacunosum-moleculare; mol, dentate molecular layer.

However, not all sites contributed equally. In all six rats, one of the recording sites contributed >40% of the correlation. Furthermore, the magnitude of correlation varied substantially across animals, presumably reflecting the variation of CA3-CA1 anatomical-functional connections sampled by the 2-dimensional probe. The prediction of CA1 power by GC recording sites was poor ($r = 0.2 \pm 0.02$) and did not increase significantly with an increasing number of sites ($p > 0.85$; ANOVA; Figure 3C).

To gain further insight into the coupling mechanism of the two hypothesized gamma oscillators, gamma current epochs with high (>0.2; such as that shown in Figures 4A and 4B) and low (<0.05) CA1-GC coherence values were grouped separately. Gamma power was significantly larger in both CA1 and GC layer sites during epochs of high coherence relative to epochs of low coherence (for all tests, $p < 0.001$; t tests), indicating that simultaneous increase of power in the two oscillators does not arise from the random coincidence of the two rhythms. Furthermore, we found that the phase difference between CA1 and GC current signals depended on the magnitude of coherence (as illustrated for a single animal in Figure 4C). During epochs of high (>0.2) coherence, the average phase difference between CA1 and GC current signals was significantly different from random (Figure 4C; $p < 0.001$; $n = 161$ pairs in six rats; Rayleigh test), with the GC source preceding the CA1 source by $38^\circ \pm 12.4^\circ$ (mean ± 2SE). These findings indicate physiological coupling between the dentate and CA3-CA1 gamma generators.

Gamma Oscillation-Related Discharge of Neurons

Tetrode recordings did not allow for the calculation of CSD, and field recordings are subject to volume-conducted contamination. Data from the probe recordings indicated that only large amplitude gamma waves (>5SD above the mean; 2% of all epochs), recorded from the GC layer, contributed to the >2 SD gamma waves in the CA1 pyramidal layer. Therefore, for all unit-field analyses, only gamma epochs (filtered: 30–80 Hz) with >2SD above the mean, recorded from the CA1 pyramidal layer, were included (trough = 0° reference). Two approaches were used to relate unit discharges to the phase of the gamma cycle. First, the discharge probability as a function of phase was calculated for each neuron, and the derived phase histograms were averaged across neurons (Figure 5A). Second, the significance of phase-locking to gamma waves was tested in every cell (Rayleigh test, $p < 0.05$), and the circular mean phases of the significantly modulated neurons were

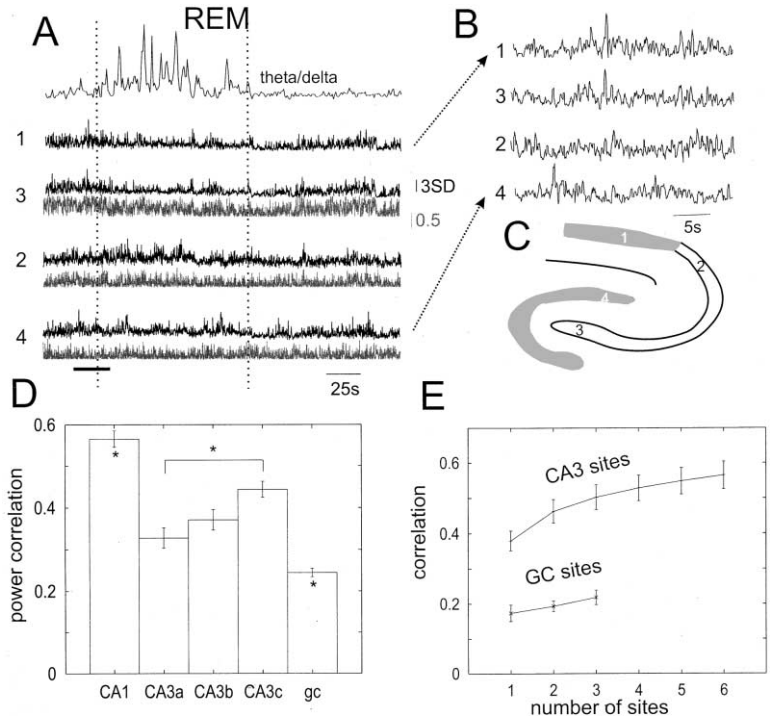

Figure 3. Dynamics of Power and Coherence Relationships across Different Regions during Sleep

(A–C) Continuous display of instantaneous gamma current power (102 ms time windows). The corresponding recording sites are indicated in (C). Uppermost trace: theta/delta ratio. REM, REM sleep episode (between dotted vertical lines). Light gray traces: coherence values between the reference (1) and other sites. The marked period in (A) (thick bar) is shown at a faster time scale in (B). Note the strong similarity of power fluctuation of gamma currents in CA1 and the CA3c site (3) and modest relationship between CA1 and GC layer (4). The strongest similarity was observed between neighboring CA1 sites (data not shown).

(D) Average correlations (r) of instantaneous power between recording sites in various subregions. Asterisks, significantly different from CA3a sites (*$p < 0.01$; ANOVA post hoc tests).

(E) Reliability of gamma current power prediction in CA1 increases with the number of recorded CA3 sites. Multiple regression was used to calculate the relationship between different sites. Gamma current power in the GC layer poorly predicted power in CA1 pyramidal layer. Group data from three rats.

used to construct frequency histograms (Figure 5B). All interneurons included in the analysis were recorded from the pyramidal layer; therefore, most of them were either basket cells or chandelier cells. These neurons provide perisomatic inhibition to the principal cells (cf. Freund and Buzsáki, 1996).

The proportion of significantly phase-locked cells was higher for interneurons in both CA1 and CA3 regions (>75%) compared to pyramidal cells (<43%; Figure 5B). CA3 interneurons ($n = 68$) fired significantly earlier (121° ± 32.4°, mean ± 95% confidence interval) than CA1 interneurons (149° ± 14.6°; $n = 53$; $p < 0.01$, Watson-Williams test), corresponding to 1.5 ms time difference at 53 Hz. The discharge probability of pyramidal neurons in the gamma cycle reached a maximum earlier than interneurons in both CA3 (64° ± 13.2°; $n = 411$ cells) and CA1 (45° ± 7.6°; $n = 294$ cells; $p < 0.02$, Watson-Williams test) regions. These phase differences translate to a 3.1 ms time difference between CA3 pyramidal cells and CA3 interneurons, 3 ms between CA3 pyramidal cells and CA1 interneurons, and 5.5 ms between CA1 pyramidal cells and CA1 interneurons. The criteria for distinguishing granule cells, interneurons, and mossy cells in the dentate gyrus are not well estab-

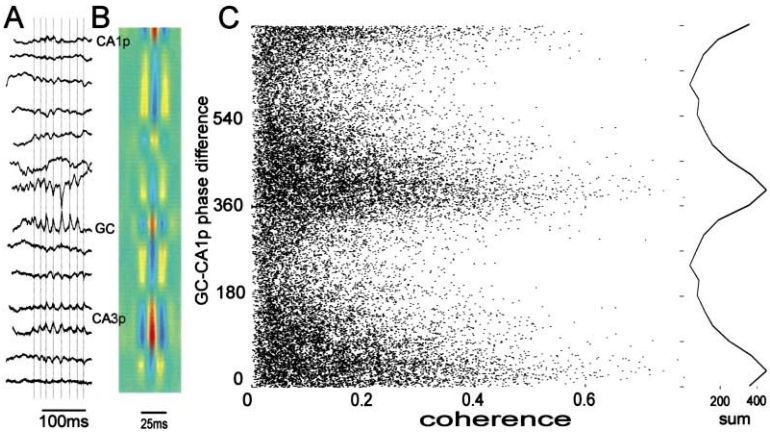

Figure 4. Synchronization of Gamma Currents in the CA1-CA3 Regions and Dentate Gyrus

(A) A short epoch of gamma oscillation (CSD traces) in the CA1-dentate axis (sink is down). The epoch was selected to show simultaneous occurrence gamma currents in all cell body layers. CA1p, CA1 pyramidal layer; CA3p, CA3 pyramidal layer; GC, granule cell layer.

(B) Averaged CSD profile of gamma currents calculated from epochs with >0.2 coherence between CA1p and GC layer sites from a 10 min recording session. Note the source-sink pairs in CA1p, GC, and CA3p.

(C) Coherence versus phase difference between gamma currents in CA1p and GC layers. Each dot represents the phase difference and coherence value between gamma epochs (102 ms) recorded at CA1p and GC layers (10 min immobility/sleep session). Two gamma cycles are shown to aid visibility. Right, sum of points. Note that maximum coherence corresponds to 30° phase difference, with GC signal leading.

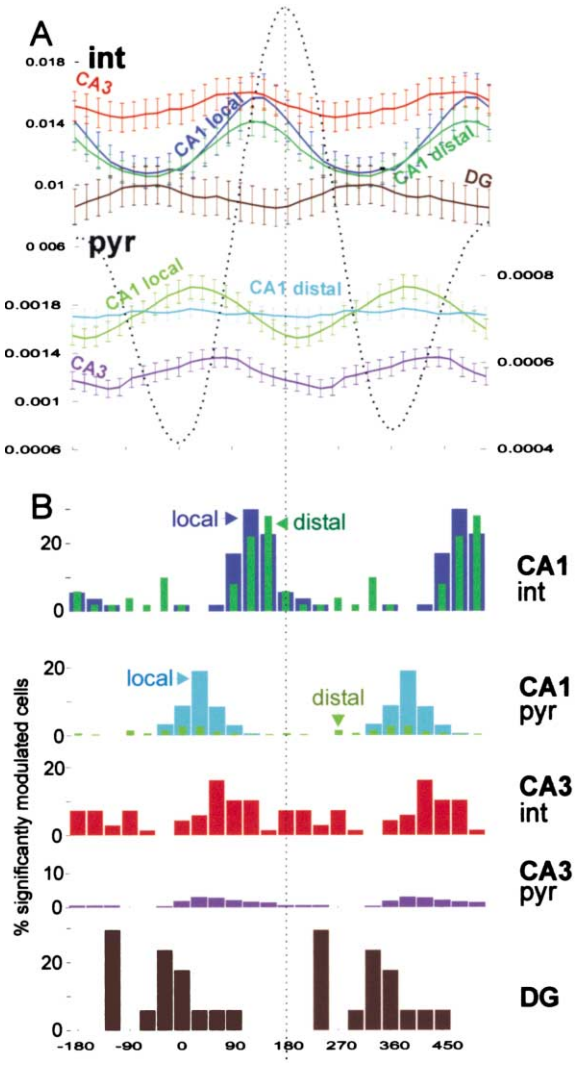

Figure 5. Phase Relationship between Gamma Field and Unit Activity

Dotted trace: wide-band (1 Hz–3 kHz) field potential averaged by gamma peaks from the reference CA1 pyramidal layer. Two cycles are shown to facilitate phase comparison with unit discharges. (A) Average discharge probability of neuronal subgroups (mean ± SE; color coded). All neurons are included, independent of the magnitude of their phase correlation with gamma oscillation. Note that CA1 pyramidal neurons (pyr) showed gamma phase modulation only with the gamma field recorded by the same tetrode (local) but not with distal (>300 μm) CA1 sites. n = 294 CA1 pyramidal cells; n = 441 CA3 pyramidal cells; n = 53 CA1 interneurons; n = 68 CA3 interneurons; n = 17 dentate gyrus (DG) neurons in six rats. (B) Phase distribution histograms of neurons with significant gamma phase modulation (see Experimental Procedures). CA1 neurons recorded by the same (local) or different (distal) tetrode than the reference gamma are shown separately. Sleep episodes and awake immobility-exploration sessions were combined for the data shown in Figures 5–8.

lished (Mizumori et al., 1989). The dentate neurons shown in Figure 5 (n = 17) were classified as putative interneurons because they had short duration spikes and autocorrelograms and firing rates with features of interneurons in CA1 (Csicsvari et al., 1999). Most of the dentate neurons were significantly phase-locked to the

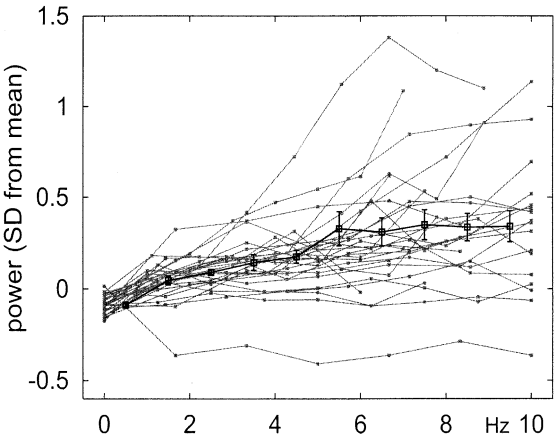

Figure 6. Relationship between Discharge Synchrony of CA1 Pyramidal Cells and the Magnitude of Locally Recorded Gamma Field Power

Horizontal axis: mean firing rate of all pyramidal cells recorded from a given tetrode in 100 ms windows. Ordinate: magnitude of gamma power, normalized as SD from the mean. Gray lines, individual tetrodes from six rats. Heavy line: mean data (±SE).

gamma waves recorded from the CA1 pyramidal layer and discharged earlier than CA3 and CA1 interneurons (Figures 5A and 5B).

We also examined the spatial coherence of unit firing during gamma oscillation. Gamma phase locking of CA1 neurons was examined separately in relation to field recorded from the same tetrode ("local" field) and to field recorded from another electrode ("distal" field, >300 μm). Correlation of CA1 pyramidal cell discharge with local field was substantially tighter than with distal fields (Figure 5A). Indeed, the mean phase histogram of unit versus distal field was virtually flat. Furthermore, the proportion of CA1 pyramidal cells with significant gamma phase locking decreased more than 3-fold with distance (from 43% local to 13% distal). In fact, the percentage of CA3 pyramidal neurons with significant phase locking to distal CA1 sites (14%) was comparable to the percentage of CA1 neurons with reliable phase locking to distal CA1 sites. In contrast, the proportion of CA1 interneurons with significant phase correlation to the gamma cycle was similar for local and distal sites (83% and 82%, respectively; Figure 5B), although when all interneurons were compared, they showed somewhat better correlation with the local than with the distal fields (Figure 5A).

The observation that the magnitude of phase locking of CA1 pyramidal neurons to gamma oscillation decreased rapidly with distance suggested that coherent EPSPs (as reflected by increased probability of spiking activity) contribute significantly to the gamma field. Indeed, in the primary visual cortex, the increased discharge of neurons in response to a preferred visual input correlates strongly with the magnitude of local gamma field oscillation (Gray et al., 1989). To further examine the unit-local field relationship in the CA1 pyramidal layer, we grouped gamma oscillations into 102 ms epochs with no detected pyramidal cell activity and an increasing degree of pyramidal cell discharge. Figure 6 illustrates that the relationship between group discharge

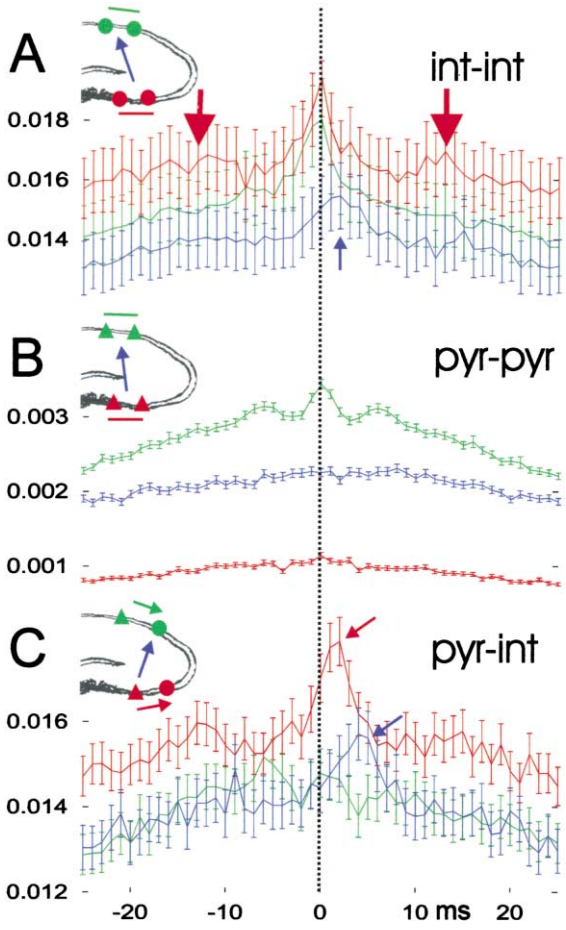

Figure 7. Unit-Unit Correlations during Gamma Oscillation

Neuron pairs in the same and different regions, recorded from different tetrodes, are shown separately (insets). (A) Interneuron pairs (circles in inset). Side peaks of CA3 interneuron pairs (n = 344 pairs) indicate gamma frequency modulation (triangles). Note the time delay (2 ms) between CA3-CA1 interneuron pairs (n = 212; arrow). CA1-CA1 pairs (n = 184). (B) Pyramidal cell pairs (n = 5300 CA1-CA1 pairs; n = 9524 CA3-CA3 pairs; n = 6618 CA3-CA1 pairs). (C) Pyramidal-interneuron pairs. Note peaks at 2 ms between CA3 pyramidal-CA3 interneuron pairs (n = 1700) and at 4–5 ms between CA3 pyramidal-CA1 interneuron pairs (n = 988). n = 964 CA1 pyramidal-CA1 interneuron pairs.

rate (pyramidal cell spikes in 102 ms windows recorded by the tetrode) and the magnitude of local gamma activity for individual sites. The group level comparison revealed a reliable and positive correlation between the discharge rate of pyramidal cells and gamma power ($r = 0.50$, $p < 0.001$).

Unit versus Unit Correlations

Cross-correlation of units at the population level provided independent support for the observations with gamma oscillations in the time and frequency domain analysis of CSD traces and unit-field correlations. Cross-correlograms between CA3-CA3 interneurons had side peaks at gamma frequency. These side peaks are less prominent in the group average (Figure 7A, arrows) because of the varying dominant frequencies in the different recording sessions. The peak of the CA3-CA1 histogram occurred at 2 ms, indicating a delay between the single CA3 and CA1 interneuron populations. When the reference event was the discharge of CA3 pyramidal cells, clear peaks were identified at 2 ms and 4–5 ms in the CA3 pyramidal-CA3 interneuron pairs and CA3 pyramidal-CA1 interneuron pairs, respectively (Figure 7C). No identifiable peak was present in the CA3-CA1 pyramidal cell pairs (Figure 7B). Taken together, these findings suggest that during gamma oscillations, CA3 pyramidal neurons contribute to the firing of target interneurons in both the CA3 and CA1 regions.

This hypothesis was investigated further by examining individual cross-correlograms. As reported previously, monosynaptic connections between CA1 pyramidal cell-interneuron pairs could be identified by a significant peak at 1–3 ms in their cross-correlograms (Csicsvari et al., 1998; Marshall et al., 2002). Putative monosynaptic connections were also observed in the CA3 region between pyramidal cell-interneuron pairs recorded by both the same (18 of 240 pairs) or different (27 of 889 pairs) tetrodes (Figure 8A). Importantly, we also identified monosynaptic connections between CA3 pyramidal cells and CA1 interneurons (8 of 495 pairs), indicated by significant peaks at 4–5 ms (Figure 8B). Finally, some CA3 interneuron pairs, recorded from two different electrodes, showed a large, significant peak in the zero bin of the cross-correlogram (n = 8; Figure 8C). Such "supersychronous" activation of interneurons (<1 ms) could have been brought about by a common input or by gap junction coupling between the interneurons (Katsumaru et al., 1988; Galarreta and Hestrin, 1999; Tamás et al., 2000; Hormuzdi et al., 2001). The incidence of electrical coupling between interneurons decreases rapidly with distance (Deans et al., 2001; Bartos et al., 2002). However, coupling between interneurons recorded by the same electrode could not be studied because the spike detection program had a refractory period of 0.6 ms.

Discussion

Our findings suggest that two gamma current generators reside in the hippocampus. The gamma oscillator in the dentate gyrus requires an extrahippocampal drive because, following surgical removal of the entorhinal cortex, the power of dentate gamma activity virtually disappears, whereas it increases several-fold in the CA1 region (Bragin et al., 1995). A similar large increase in CA1 gamma power has been described after transient impairment of the entorhinal cortex following afterdischarges (Leung 1987). Furthermore, the discharge frequency of layer II, III entorhinal cortical neurons is increased during theta-associated behaviors (Chrobak and Buzsáki, 1998), which may contribute to the selectively increased gamma current power in the dentate gyrus during theta relative to nontheta epochs. In contrast to the dentate oscillator, gamma rhythm generation in the CA3-CA1 regions does not require external inputs. The dentate and CA3-CA1 generators can be coupled under physiological conditions as indicated by (1) phase-locked discharge of putative dentate interneurons to CA1 gamma waves, (2) the weak but significant correlation of gamma power in CA1 and GC layers, and

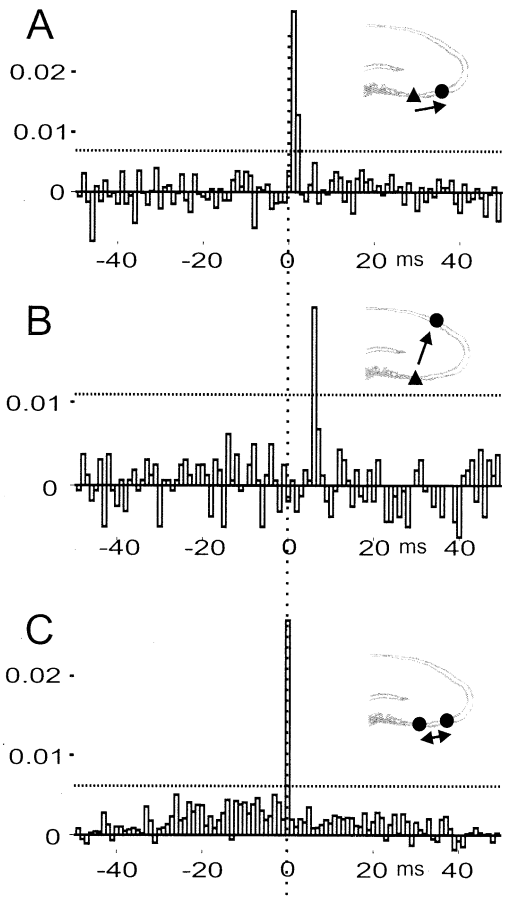

Figure 8. Monosynaptic Activation of Interneurons

Monosynaptic discharge of a CA3 interneuron (A) or CA1 interneuron (B) by CA3 pyramidal cells. (A) and (B) are different cell pairs. Shuffling-corrected cross-correlograms indicate significant (dotted lines, 3 SD, $p < 0.002$) peaks at 1 and 6 ms, respectively. Ordinate: probability of interneuron discharge. 45 of 1129 CA3 pyramidal cell-CA3 interneuron pairs and 8 of 495 CA3 pyramidal cell-CA1 interneuron pairs showed significant peaks at monosynaptic latency. (C) Shuffling-corrected cross-correlogram between two interneurons, recorded by two nearby tetrodes. Note the large, significant peak at time 0 ms. 8 such pairs (out of 344 possible pairs) were identified. Simultaneous activation of the interneurons can be brought about by either a common input or gap junction connections between interneurons.

(3) the phase-lead of GC gamma currents relative to CA1. On average, the two oscillators are weakly synchronized, and the strength of coupling fluctuates over a wide range. The precise behavioral conditions that specifically enhance the coherence between the gamma oscillators at the input and output stages of the hippocampus remain to be uncovered.

CA3-CA1 Regions Sustain Gamma Oscillation

Various in vivo, in vitro, and computational models have been put forward for the explanation of the emergence of gamma frequency oscillations in cortical structures (Leung, 1982; Whittington et al., 1995; Traub et al., 1996, 1997, 1999, 2001; Wang and Buzsáki, 1996; Chow et al., 1998; Fisahn et al., 1998, 2002; White et al., 1998; Fellous and Sejnowski, 2000; Gray, 1994; Kopell et al., 2000; Bracci et al., 1999; Colling et al., 1998; Stanford et al., 1998). We suggest that the following model can account best for our observations (Figure 9). We propose that intrahippocampally generated gamma activity results from the interaction of CA3 pyramidal neurons and interneurons and that the coherent coupling of the oscillating cell groups is responsible for the extracellular gamma fields.

A critical test of a model is to explain the spike time relationships between participating neurons and the field currents they produce. In our experiments, phase-reversed gamma fields and associated source-sink pairs were present in the strata pyramidale and radiatum of both CA3 and CA1 regions. The timing between pyramidal cells and putative basket/chandelier interneurons, however, was different in the two regions, suggesting that the network mechanisms of gamma generation are not identical in CA3 and CA1. In the CA3 region, peak activity of the pyramidal cell population preceded the peak of CA3 interneuron discharges by approximately 2 ms, measured either by unit-unit correlations or by comparing peak discharges relative to the reference gamma cycle in CA1 pyramidal layer. The discharging pyramidal cells and interneurons can therefore provide dendritic excitation and somatic inhibition of pyramidal cells. These events are suggested to give rise to the sink-source pair in strata radiatum and pyramidale. Although we do not have direct measurements of EPSPs and IPSPs, the timing scenario of unit discharges and field potentials observed here is quite similar to that described in the hippocampal slice during carbachol-induced gamma oscillation and in an associated computational model (Fisahn et al., 1998; Traub et al., 2000). In the slice experiment, the peak EPSC coincided with the trough in stratum radiatum (peak in pyramidal layer) followed by the peak IPSC 2–3 ms (i.e., 30°–60°) later. Thus, observations in vitro and in vivo are in agreement in the CA3 region, and the mechanisms suggested from the in vitro observations may apply to the intact hippocampus (Figure 9).

We suggest further that the gamma phase-locked discharge of CA3 pyramidal cells is responsible for gamma oscillations in the CA1 region as well. First, recordings from multiple CA3 sites predicted CA1 gamma power better than any single site. Second, in previous in vitro experiments, surgical lesion between the two regions eliminated carbachol-induced gamma oscillation in CA1 but left it intact in CA3 (Fisahn et al., 1998). Third, the sink-source distribution of gamma oscillation in the CA1 region was similar to the CSD profile evoked by stimulation of the commissural/associational affferents (data not shown). Fourth, the time difference between sources in the CA3 and CA1 pyramidal layers, measured by both time and frequency domain analyses, is in register with the time difference between discharging CA3 and CA1 interneurons, calculated by both unit versus gamma field and unit versus unit correlations. Nevertheless, CA3 pyramidal neurons are not the immediate cause of gamma-related discharge of CA1 pyramidal cells, because the peak of CA1 pyramidal cell activity occurred earlier than the peak in CA3 and at times when CA1 interneuron activity was at its minimum. We hypothesize that the gamma cycle-related sink-source pair in CA1 strata radiatum and pyramidale corresponds to EPSPs

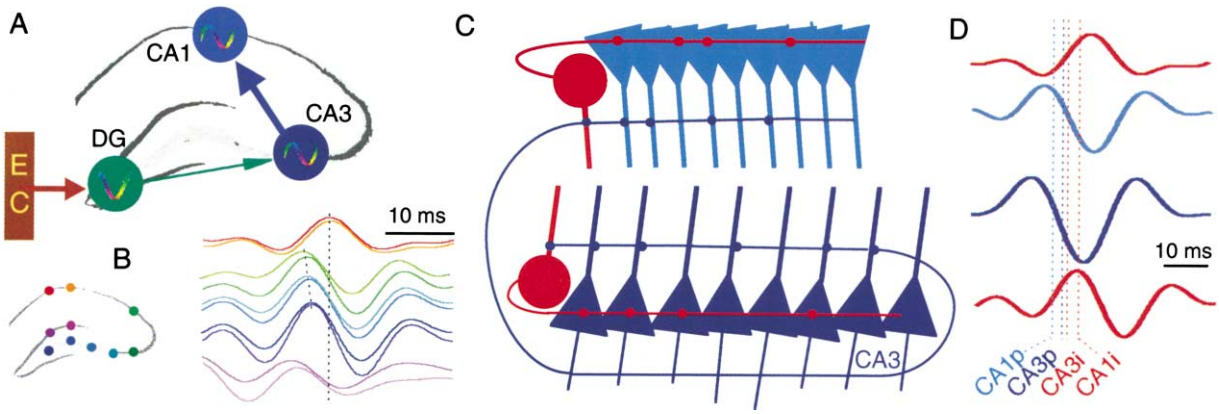

Figure 9. Proposed Mechanism of Gamma Oscillations

(A) Two major gamma oscillators are postulated. The oscillator in the dentate gyrus (DG) depends on an extrahippocampal input from the entorhinal cortex (EC). The CA3 circuit represents an intrahippocampal gamma oscillator. CA1 gamma depends primarily on CA3 input. The DG and CA3 gamma oscillators are weakly coupled. Direct influence of the EC input on the intrahippocampal (CA3) gamma oscillator is not shown.

(B) Averaged gamma field activity (voltage) recorded from the CA1 and CA3 pyramidal layers and GC layer. Recording sites and traces are color coded. The reference site was in the CA1 pyramidal layer. Note gradual latency shift in the CA3a, b, c direction (oblique dotted line).

(C) Discharging CA3 pyramidal neurons excite each other and discharge basket and chandelier cells in both CA3 and CA1 regions. Feedforward inhibition prevents CA1 pyramidal cells from discharging.

(D) Averaged gamma current activity in the CA1 strata pyramidale and radiatum (upper two traces) and in the CA3 strata radiatum and pyramidale (bottom two traces). Preferred phases of pyramidal cells (CA1p, CA3p) and interneurons (CA3i, CA1i) are indicted by dotted lines. Extracellular gamma fields are assumed to derive from ensuing EPSPs and IPSPs in the dendritic and somatic regions, respectively.

(sink) and disynaptic IPSPs (source) in the dendrites and somata of CA1 pyramidal cells, brought about by the phase-locked discharge of CA3 pyramidal neurons. Under average conditions, feedforward inhibition appears to curtail the excitatory drive of CA1 pyramidal cells.

The inability of the CA1 region to generate gamma oscillations on its own may be due to the absence of an excitatory recurrent collateral system, the hallmark of the CA3 region or other hitherto unidentified differences between the two regions. Although CA1 pyramidal cells are known to discharge their interneurons (Ali et al., 1998; Csicsvari et al., 1998; Marshall et al., 2002), the long time difference between the peak discharge of CA1 pyramidal cells and interneurons (104°, i.e., >5 ms) is in favor of the interpretation that the CA3 output is the major source of gamma cycle-related discharge of CA1 basket cells. Furthermore, CA1 basket cells receive many more synapses from CA3 than from CA1 pyramidal cells (cf. Freund and Buzsáki, 1996). Other postulated mechanisms of gamma oscillations, such as mutual interactions among interneurons via both inhibitory synapses and gap junctions (Whittington et al., 1995; Wang and Buzsáki, 1996; Tamás et al., 2000; Hormuzdi et al., 2001; Deans et al., 2001; Traub et al., 1996, 1997, 2000, 2001) or feedback inhibition (Leung, 1979, 1998; Lisman, 1998), may also contribute to the above suggested mechanisms. The 0 ms discharge of interneuron pairs observed in the present experiments is in support of the suggestion that gap junctions may assist gamma oscillations.

Our experiments also revealed functional differences within the CA3 region. The correlation of current power was better between CA1 and CA3c sites than between the spatially more proximal CA1-CA3a sites. Similarly, gamma coherence between CA1 and CA3c sites was higher than between CA1-CA3a sites. It should be noted here that in the curved portion of CA3b (fimbrial), the absolute current power is not reflected faithfully because of the vertical positioning of the recording sites. Nevertheless, this does not affect the power variation or coherence measurements. Finally, the latency between gamma cycle peaks recorded in CA1 and CA3 regions decreased in the CA3a, b, and c direction (Figure 9B). These observations can be attributed to the differential connectivity of the CA3 subregions. Most axon collaterals of CA3c pyramidal cells innervate CA1 neurons. The ratio of recurrent collaterals versus CA1 projecting axons of CA3 pyramidal neurons increases progressively in the CA3 c, b, a axis (Li et al., 1994). We hypothesize that intrahippocampal gamma oscillation emanates from the recurrent collateral-dense CA3a-b subregions, whose activity recruits CA3c, which, in turn, entrains CA1 neurons.

Gamma Frequency Synchrony of Active Principal Cells

Axon terminals of single CA3 pyramidal neurons cover as much as two thirds of the longitudinal extent of the CA1 region (Ishizuka et al., 1990; Li et al., 1994). On the basis of anatomy alone, therefore, one would expect a highly coherent gamma activity throughout the entire CA1 region. Indeed, interneurons at distal locations were highly coupled with each other as well as with both local and distal fields. In contrast to this expectation, a rapid decrease in pyramidal cell versus gamma wave coupling with distance was observed. This may be so because EPSPs may also significantly contribute to the gamma field (Leung, 1979; 1982; Eeckman and Freeman, 1990; Fisahn et al., 1998, 2002). Although we did not measure EPSPs directly, we could indirectly assess their magni-

tude by the discharge probability of pyramidal cells. Increased discharge probability of pyramidal neurons was correlated with increased local gamma power, similar to the relationship between stimulus-driven unit activity and increased amplitude of gamma oscillation in the primary visual cortex (Gray et al., 1989). Because very few hippocampal pyramidal cells are active in the time window of the gamma cycle during spatial behavior (O'Keefe and Nadel, 1978; Csicsvari et al., 1999; Henze et al., 2000; Redish et al., 2001; Hirase et al., 2001), our prediction is that gamma current power at recording sites with active place neurons correlates with the spatial location of the animal. Similarly, temporally coordinated discharge of place cells at different locations may be accompanied by an increased coherence between the locally recorded gamma currents. The postulated granularity of gamma coherence is further supported by the observation that a single CA3 site was nearly as good a predictor of CA1 gamma power at a given location as the sum of the remaining sites.

Experimental Procedures

The general surgical procedures, electrode preparation, implantation, and spike sorting methods have been described (Csicsvari et al., 1998, 1999, 2000). All procedures conformed to the NIH Guide for the Care and Use of Laboratory Animals. In short, 12 male rats of the Sprague-Dawley strain (400–900 g) were anesthetized with a mixture (4 ml/kg) of ketamine (25 mg/ml), xylazine (1.3 mg/ml), and acepromazine (0.25 mg/ml) and placed in the stereotaxic apparatus. Six animals were implanted with silicon probes, and the remaining six animals with wire tetrodes. The silicon probes contained six shanks (300 μm shank separation) and each shank had 16 recording sites (108 μm^2) with 100 μm vertical spacing. The probes were implanted at anterior-posterior, AP = −3.5 mm, and medio-lateral, ML = 2.5 mm, position. During the experiment, the probe was moved gradually, and recordings were made at each depth location. A pair of stainless steel wires (60 μm in diameter) was placed into the fimbria-fornix/hippocampal commissure (AP = −0.8, L = 0.5, V = −4.2 mm) to stimulate the commissural afferents to the CA1 region and another pair in the angular bundle (AP = −7.0, L = 4.5, V = −3.5 mm) to stimulate the entorhinal input. The evoked responses by these pathways helped the on-line identification of the recording electrodes (Bragin et al., 1995). The remaining animals were implanted with wire tetrodes (four 13 μm enamel-coated nichrome wires) (Gray et al., 1995). The "tetrodes" were attached to a multidrive array, and eight electrodes were independently moved during the experiment. The physiological data were collected during spontaneous exploration, immobility states, and slow wave sleep and REM sleep episodes in the home cage. Instrumentation amplifiers built into the female connector (Szabó et al., 2001) were used to reduce cable movement artifacts. Two synchronized 64-channel DataMax systems (16-bit resolution; RC Electronics, Santa Barbara, CA) continuously recorded electrical activity at 20 kHz to computer hard disk.

Spike Sorting

The continuously recorded wide-band signals were high-pass filtered (0.8–5 kHz) digitally. Units were identified and isolated by a semiautomatic "cluster cutting" algorithm (Csicsvari et al., 1998; Harris et al., 2000). Auto- and cross-correlations were calculated to verify the clustering procedure.

CSD Analysis

One-dimensional CSD maps were calculated in one direction (depth) as the second spatial derivative of the local field potentials (Bragin et al., 1995). This approach assumes that the resistivity of the extracellular medium is similar at different depths. Although some resistivity differences are present in the different hippocampal layers, in practice these are not large enough to significantly modify the spatial distribution of sinks and sources (Holsheimer, 1987). CSD transformation was carried out on the averaged field response. For averaging, a reference electrode was chosen (either the CA1 pyramidal layer or the granule cell layer), and peaks of gamma cycles, 2 SD above the overall background power, were detected. The choice of reference this way is biased to detect CSD of the signals coherent with the events close to the reference site.

Detection of Gamma and Theta Patterns

For the extraction of gamma oscillatory periods, the wide band (1 Hz–5 kHz) recorded data were digitally filtered (30–80 Hz). The digital filtering reliably excluded ripple (140–200 Hz) epochs. The power (root mean square) of the filtered signal was calculated for each electrode within a 25 ms window. The mean and SD of power of a given file were first calculated to determine the detection threshold. Gamma oscillatory periods with a power of 2 SD above the mean were detected and used for subsequent analysis. The beginning and the end of oscillatory periods were marked by time points at which the power decreased $<$1 SD. These gamma epochs represented approximately 10% of the 10–15 min recording sessions. Peaks and troughs of individual gamma cycles ($>$2 SD) were detected. Theta epochs during exploration and REM sleep were detected by calculating the ratio of the theta (5–10 Hz) and delta (2–4 Hz) frequency band in 2.0 s windows, followed by manual adjustment. A Hamming window was used during the power spectral calculations. After digital filtering (5–28 Hz), the negative peaks of individual theta waves were identified (Csicsvari et al., 1999; J. Csicsvari et al., 2001, Soc. Neurosci., abstract).

Spectral Analysis

Coherence and spectral phase differences were calculated in successive 102.4 ms (512 samples) windows. Hamming windows were used during the power spectrum estimations. For the estimation of coherence and spectral phase difference within short time segments (e.g., Figures 3 and 4), Thomson's multitaper method was used (Thomson, 1982; Mitra and Pesaran, 1999). Circular standard errors were calculated for spectral phase differences (Fisher, 1993).

Field-Unit and Unit-Unit Correlations

The phase relationship between unit activity and gamma oscillation was calculated by the following manner. Each spike was assigned to a given phase (bin size of 20°) of the normalized gamma cycle, and a phase histogram was calculated by summing unit discharges that occurred at different phases. Phase histograms were normalized by dividing each bin by the number of gamma cycles, and the probability of unit discharge at each phase was computed. Circular statistics of the unit-discharge gamma phases (i.e., Rayleigh test, $p < 0.05$) (Kanji, 1999) were used to test whether individual units showed significant phase locking to gamma waves. The Watson-Williams circular test was used to quantify differences of phase locking between neuron populations (Kanji, 1999). Cross-correlation histograms of unit discharges were calculated to assess monosynaptic connections between units, as described in Csicsvari et al. (1998).

Prediction of CA1 Gamma Power Based on CA3 and Dentate Gamma Activity

Gamma power was estimated in consecutive 200 ms windows in the CA1 pyramidal layer based on gamma power at multiple sites in the CA3 or GC layers. For these calculations, cross-validation procedure was used; i.e., the regression equation was established based on the first half of the recordings, and the correlation coefficient was calculated for the second half. All possible combinations of CA3 and GC sites were used to calculate the average correlation coefficient (Csicsvari et al., 2000).

Histological Procedures

Following completion of the experiments, the rats were deeply anesthetized and perfused through the heart, first with 0.9% saline solution followed by a 10% buffered formalin phosphate solution. The brains were sectioned by a Vibroslice at 100 μm in the coronal plane. The sections were mounted on slides, Nissl stained, and coverslipped. The tracks of the tetrodes or silicon probes were

reconstructed from multiple sections. The exact recording sites in the vertical direction for each session were determined by the evoked responses. The derived electrical patterns then were superimposed on the anatomical substrate that emanated them (e.g., Figure 1).

Acknowledgments

We thank D. Buhl, G. Dragoi, K. Harris, D. Henze, N. Kopell, L.S. Leung, A. Sirota, and the anonymous referees for their constructive comments on the manuscript. This work was supported by the NIH (NS34994, NS43157; MH54671; 1P41RR09754).

Received: July 10, 2002
Revised: November 26, 2002

References

Ali, A.B., Deuchars, J., Pawelzik, H., and Thomson, A.M. (1998). CA1 pyramidal to basket and bistratified cell EPSPs: dual intracellular recordings in rat hippocampal slices. J. Physiol. *507*, 201–217.

Bartos, M., Vida, I., Frotscher, M., Meyer, A., Monyer, H., Geiger, J.R., and Jonas, P. (2002). Fast synaptic inhibition promotes synchronized gamma oscillations in hippocampal interneuron networks. Proc. Natl. Acad. Sci. USA *99*, 13222–13227.

Bracci, E., Vreugdenhil, M., Hack, S.P., and Jefferys, J.G. (1999). On the synchronizing mechanisms of tetanically induced hippocampal oscillations. J. Neurosci. *19*, 8104–8113.

Bragin, A., Jandó, G., Nadasdy, Z., Hetke, J., Wise, K., and Buzsáki, G. (1995). Gamma (40–100 Hz) oscillation in the hippocampus of the behaving rat. J. Neurosci. *15*, 47–60.

Bullock, T.H., and McClune, M.C. (1989). Lateral coherence of the electrocorticogram: a new measure of brain synchrony. Electroencephalogr. Clin. Neurophysiol. *73*, 479–498.

Buzsáki, G., Leung, L.W., and Vanderwolf, C.H. (1983). Cellular bases of hippocampal EEG in the behaving rat. Brain Res. *287*, 139–171.

Buzsáki, G., Llinás, R., Berthoz, A., and Christen, Y. (1994). Temporal Coding in the Brain (Berlin: Springer-Verlag).

Charpak, S., Paré, D., and Llinás, R. (1995). The entorhinal cortex entrains fast CA1 hippocampal oscillations in the anaesthetized guinea-pig: role of the monosynaptic component of the perforant path. Eur. J. Neurosci. *7*, 1548–1557.

Chow, C., White, J., Ritt, J., and Kopell, N. (1998). Frequency control in synchronous networks of inhibitory neurons. J. Comput. Neurosci. *5*, 407–420.

Chrobak, J.J., and Buzsáki, G. (1998). Gamma oscillations in the entorhinal cortex of the freely behaving rat. J. Neurosci. *18*, 388–398.

Colling, S.B., Stanford, I.M., Traub, R.D., and Jefferys, J.G. (1998). Limbic gamma rhythms. I. Phase-locked oscillations in hippocampal CA1 and subiculum. J. Neurophysiol. *80*, 155–161.

Csicsvari, J., Hirase, H., Czurkó, A., and Buzsáki, G. (1998). Reliability and state dependence of pyramidal cell-interneuron synapses in the hippocampus: an ensemble approach in the behaving rat. Neuron *21*, 179–189.

Csicsvari, J., Hirase, H., Czurkó, A., Mamiya, A., and Buzsáki, G. (1999). Oscillatory coupling of hippocampal pyramidal cells and interneurons in the behaving rat. J. Neurosci. *19*, 274–287.

Csicsvari, J., Hirase, H., Mamiya, A., and Buzsáki, G. (2000). Ensemble patterns of hippocampal CA3-CA1 neurons during sharp wave-associated population events. Neuron *28*, 585–594.

Deans, M.R., Gibson, J.R., Sellitto, C., Connors, B.W., and Paul, D.L. (2001). Synchronous activity of inhibitory networks in neocortex requires electrical synapses containing connexin36. Neuron *31*, 477–485.

Eckhorn, R. (1994). Oscillatory and non-oscillatory synchronizations in the visual cortex and their possible roles in associations of visual features. Prog. Brain Res. *102*, 405–426.

Eeckman, F.H., and Freeman, W.J. (1990). Correlations between unit firing and EEG in the rat olfactory system. Brain Res. *528*, 238–244.

Engel, A.K., Fries, P., and Singer, W. (2001). Dynamic predictions: oscillations and synchrony in top-down processing. Nat. Rev. Neurosci. *2*, 704–716.

Fell, J., Klaver, P., Lehnertz, K., Grunwald, T., Schaller, C., Elger, C.E., and Fernandez, G. (2001). Human memory formation is accompanied by rhinal-hippocampal coupling and decoupling. Nat. Neurosci. *4*, 1159–1160.

Fellous, J.M., and Sejnowski, T.J. (2000). Cholinergic induction of oscillations in the hippocampal slice in the slow (0.5–2 Hz), theta (5–12 Hz), and gamma (35–70 Hz) bands. Hippocampus *10*, 187–197.

Fetz, E.E., Chen, D., Murthy, V.N., and Matsumura, M. (2000). Synaptic interactions mediating synchrony and oscillations in primate sensorimotor cortex. J. Physiol. (Paris) *94*, 323–331.

Fisahn, A., Pike, F.G., Buhl, E.H., and Paulsen, O. (1998). Cholinergic induction of network oscillations at 40 Hz in the hippocampus in vitro. Nature *394*, 186–189.

Fisahn, A., Yamada, M., Duttaroy, A., Gan, J.W., Deng, C.X., McBain, C.J., and Wess, J. (2002). Muscarinic induction of hippocampal gamma oscillations requires coupling of the M1 receptor to two mixed cation currents. Neuron *33*, 615–624.

Fisher, N.I. (1993). Statistical Analysis of Circular Data (Cambridge, UK: Cambrige Univeristy Press).

Freund, T.F., and Buzsáki, G. (1996). Interneurons of the hippocampus. Hippocampus *6*, 347–470.

Fries, P., Reynolds, J.H., Rorie, A.E., and Desimone, R. (2001a). Modulation of oscillatory neuronal synchronization by selective visual attention. Science *291*, 1560–1563.

Fries, P., Neuenschwander, S., Engel, A.K., Goebel, R., and Singer, W. (2001b). Rapid feature selective neuronal synchronization through correlated latency shifting. Nat. Neurosci. *4*, 194–200.

Galarreta, M., and Hestrin, S. (1999). A network of fast-spiking cells in the neocortex connected by electrical synapses. Nature *402*, 72–75.

Gray, C.M. (1994). Synchronous oscillations in neuronal systems: mechanisms and functions. J. Comput. Neurosci. *1–2*, 11–38.

Gray, C.M., Konig, P., Engel, A.K., and Singer, W. (1989). Oscillatory responses in cat visual cortex exhibit inter-columnar synchronization which reflects global stimulus properties. Nature *338*, 334–337.

Gray, C.M., Maldonado, P.E., Wilson, M., and McNaughton, B. (1995). Tetrodes markedly improve the reliability and yield of multiple single- unit isolation from multi-unit recordings in cat striate cortex. J. Neurosci. Methods *63*, 43–54.

Harris, K.D., Henze, D.A., Csicsvari, J., Hirase, H., and Buzsáki, G. (2000). Accuracy of tetrode spike separation as determined by simultaneous intracellular and extracellular measurements. J. Neurophysiol. *84*, 401–414.

Hasselmo, M.E., Wyble, B.P., and Wallenstein, G.V. (1996). Encoding and retrieval of episodic memories: role of cholinergic and GABAergic modulation in the hippocampus. Hippocampus *6*, 693–708.

Henze, D.A., Borhegyi, Z., Csicsvari, J., Mamiya, A., Harris, K.D., and Buzsáki, G. (2000). Intracellular features predicted by extracellular recordings in the hippocampus in vivo. J. Neurophysiol. *84*, 390–400.

Hirai, N., Uchida, S., Maehara, T., Okubo, Y., and Shimizu, H. (1999). Enhanced gamma (30–150 Hz) frequency in the human medial temporal lobe. Neuroscience *90*, 1149–1155.

Hirase, H., Leinekugel, X., Csicsvari, J., Czurkó, A., and Buzsáki, G. (2001). Behavior-dependent states of the hippocampal network affect functional clustering of neurons. J. Neurosci. *21*, RC145.

Holsheimer, J. (1987). Electrical conductivity of the hippocampal CA1 layers and application to current-source-density analysis. Exp. Brain Res. *67*, 402–410.

Hormuzdi, S.G., Pais, I., LeBeau, F.E., Towers, S.K., Rozov, A., Buhl, E.H., Whittington, M.A., and Monyer, H. (2001). Impaired electrical signaling disrupts gamma frequency oscillations in connexin 36-deficient mice. Neuron *31*, 487–495.

Ishizuka, N., Weber, J., and Amaral, D.G. (1990). Organization of intrahippocampal projections originating from CA3 pyramidal cells in the rat. J. Comp. Neurol. *295*, 580–623.

Jensen, O., and Lisman, J.E. (1996). Theta/gamma networks with

slow NMDA channels learn sequences and encode episodic memory: role of NMDA channels in recall. Learn. Mem. *3*, 264–278.

Kanji, G.K. (1999). 100 Statistical Tests (London: SAGE Publications).

Katsumaru, H., Kosaka, T., Heizmann, C.W., and Hama, K. (1988). Gap junctions on GABAergic neurons containing the calcium-binding protein parvalbumin in the rat hippocampus (CA1 region). Exp. Brain Res. *72*, 363–370.

Kopell, N., Ermentrout, G.B., Whittington, M.A., and Traub, R.D. (2000). Gamma rhythms and beta rhythms have different synchronization properties. Proc. Natl. Acad. Sci. USA *97*, 1867–1872.

Leung, S.W. (1979). Potentials evoked by alvear tract in hippocampal CA1 region of rats. II. Spatial field analysis. J. Neurophysiol. *42*, 1571–1589.

Leung, L.S. (1982). Nonlinear feedback model of neuronal populations in hippocampal CAl region. J. Neurophysiol. *47*, 845–868.

Leung, L.W. (1987). Hippocampal electrical activity following local tetanization. I. After discharges. Brain Res. *419*, 173–187.

Leung, L.S. (1992). Fast (beta) rhythms in the hippocampus: a review. Hippocampus *2*, 93–98.

Leung, L.S. (1998). Generation of theta and gamma rhythms in the hippocampus. Neurosci. Biobehav. Rev. *22*, 275–290.

Li, X.G., Somogyi, P., Ylinen, A., and Buzsáki, G. (1994). The hippocampal CA3 network: an in vivo intracellular labeling study. J. Comp. Neurol. *339*, 181–208.

Lisman, J. (1998). What makes the brain's tickers tock. Nature *394*, 132–133.

Lisman, J.E., and Idiart, M.A. (1995). Storage of 7 +/− 2 short-term memories in oscillatory subcycles. Science *267*, 1512–1515.

Llinás, R., Ribary, U., Contreras, D., and Pedroarena, C. (1998). The neuronal basis for consciousness. Philos. Trans. R. Soc. Lond. B Biol. Sci. *353*, 1841–1849.

Marshall, L., Henze, D.A., Hirase, H., Leinekugel, X., Dragoi, G., and Buzsáki, G. (2002). Hippocampal pyramidal cell-interneuron spike transmission is frequency dependent and responsible for place modulation of interneuron discharge. J. Neurosci. *22*, RC197.

Mitra, P.P., and Pesaran, B. (1999). Analysis of dynamic brain imaging data. Biophys. J. *76*, 691–708.

Mizumori, S.J., McNaughton, B.L., and Barnes, C.A. (1989). A comparison of supramammillary and medial septal influences on hippocampal field potentials and single-unit activity. J. Neurophysiol. *61*, 15–31.

O'Keefe, J., and Nadel, L. (1978). Hippocampus as a Cognitive Map (Oxford: Clarendon).

Orban, G., Kiss, T., Lengyel, M., and Erdi, P. (2001). Hippocampal rhythm generation: gamma-related theta-frequency resonance in CA3 interneurons. Biol. Cybern. *84*, 123–132.

Penttonen, M., Kamondi, A., Acsady, L., and Buzsáki, G. (1998). Gamma frequency oscillation in the hippocampus of the rat: intracellular analysis in vivo. Eur. J. Neurosci. *10*, 718–728.

Redish, A.D., Battaglia, F.P., Chawla, M.K., Ekstrom, A.D., Gerrard, J.L., Lipa, P., Rosenzweig, E.S., Worley, P.F., Guzowski, J.F., McNaughton, B.L., et al. (2001). Independence of firing correlates of anatomically proximate hippocampal pyramidal cells. J. Neurosci. *21*, RC134.

Roelfsema, P.R., Engel, A.K., Konig, P., and Singer, W. (1997). Visuomotor integration is associated with zero time-lag synchronization among cortical areas. Nature *385*, 157–161.

Rolls, E.T. (1996). A theory of hippocampal function in memory. Hippocampus *6*, 601–620.

Singer, W. (1993). Synchronization of cortical activity and its putative role in information processing and learning. Annu. Rev. Physiol. *55*, 349–374.

Soltész, I., and Déschenes, M. (1993). Low- and high-frequency membrane potential oscillations during theta activity in CA1 and CA3 pyramidal neurons of the rat hippocampus under ketamine-xylazine anesthesia. J. Neurophysiol. *70*, 97–116.

Stanford, I.M., Traub, R.D., and Jefferys, J.G. (1998). Limbic gamma rhythms. II. Synaptic and intrinsic mechanisms underlying spike doublets in oscillating subicular neurons. J. Neurophysiol. *80*, 162–171.

Stenkamp, K., Palva, J.M., Uusisaari, M., Schuchmann, S., Schmitz, D., Heinemann, U., and Kaila, K. (2001). Enhanced temporal stability of cholinergic hippocampal gamma oscillations following respiratory alkalosis in vitro. J. Neurophysiol. *85*, 2063–2069.

Stumpf, C. (1965). Drug action on the electrical activity of the hippocampus. Int. Rev. Neurobiol. *8*, 77–138.

Szabó, I., Czurkó, A., Csicsvari, J., Hirase, H., Leinekugel, X., and Buzsáki, G. (2001). The application of printed circuit board technology for fabrication of multi-channel micro-drives. J. Neurosci. Methods *105*, 105–110.

Tamamaki, N., and Nojyo, Y. (1993). Projection of the entorhinal layer II neurons in the rat as revealed by intracellular pressure-injection of neurobiotin. Hippocampus *3*, 471–480.

Tamás, G., Buhl, E.H., Lorincz, A., and Somogyi, P. (2000). Proximally targeted GABAergic synapses and gap junctions synchronize cortical interneurons. Nat. Neurosci. *3*, 366–371.

Thomson, D.J. (1982). Spectrum estimation and harmonic analysis. Proc. IEEE. *70*, 1055–1096.

Tiesinga, P.H., Fellous, J.M., Jose, J.V., and Sejnowski, T.J. (2001). Computational model of carbachol-induced delta, theta, and gamma oscillations in the hippocampus. Hippocampus *11*, 251–274.

Towers, S.K., LeBeau, F.E., Gloveli, T., Traub, R.D., Whittington, M.A., and Buhl, E.H. (2002). Fast network oscillations in the rat dentate gyrus in vitro. J. Neurophysiol. *87*, 1165–1168.

Traub, R.D., Whittington, M.A., Stanford, I.M., and Jefferys, J.G. (1996). A mechanism for generation of long-range synchronous fast oscillations in the cortex. Nature *383*, 621–624.

Traub, R.D., Jefferys, J.G., and Whittington, M.A. (1997). Simulation of gamma rhythms in networks of interneurons and pyramidal cells. J. Comput. Neurosci. *4*, 141–150.

Traub, R.D., Jefferys, J.G., and Whittington, M.A. (1999). Fast Oscillations in Cortical Circuits (Cambridge, MA: MIT Press).

Traub, R.D., Bibbig, A., Fisahn, A., LeBeau, F.E., Whittington, M.A., and Buhl, E.H. (2000). A model of gamma-frequency network oscillations induced in the rat CA3 region by carbachol in vitro. Eur. J. Neurosci. *12*, 4093–4106.

Traub, R.D., Kopell, N., Bibbig, A., Buhl, E.H., LeBeau, F.E., and Whittington, M.A. (2001). Gap junctions between interneuron dendrites can enhance synchrony of gamma oscillations in distributed networks. J. Neurosci. *21*, 9478–9486.

Varela, F., Lachaux, J.P., Rodriguez, E., and Martinerie, J. (2001). The brainweb: phase synchronization and large-scale integration. Nat. Rev. Neurosci. *2*, 229–239.

Wallenstein, G.V., and Hasselmo, M.E. (1997). GABAergic modulation of hippocampal population activity: sequence learning, place field development, and the phase precession effect. J. Neurophysiol. *78*, 393–408.

Wang, X.J., and Buzsáki, G. (1996). Gamma oscillation by synaptic inhibition in a hippocampal interneuronal network model. J. Neurosci. *16*, 6402–6413.

White, J., Chow, C., Ritt, J., Soto-Trevino, C., and Kopell, N. (1998). Synchronization and oscillatory dynamics in heterogeneous, mutually inhibited neurons. J. Comput. Neurosci. *5*, 5–16.

Whittington, M.A., Traub, R.D., and Jefferys, J.G. (1995). Synchronized oscillations in interneuron networks driven by metabotropic glutamate receptor activation. Nature *373*, 612–615.

Whittington, M.A., Traub, R.D., Faulkner, H.J., Stanford, I.M., and Jefferys, J.G. (1997). Recurrent excitatory postsynaptic potentials induced by synchronized fast cortical oscillations. Proc. Natl. Acad. Sci. USA *94*, 12198–12203.

Whittington, M.A., Doheny, H.C., Traub, R.D., LeBeau, F.E., and Buhl, E.H. (2001). Differential expression of synaptic and nonsynaptic mechanisms underlying stimulus-induced gamma oscillations in vitro. J. Neurosci. *21*, 1727–1738.